Chang *et al. Miner Miner Mater* 2022;1:6
DOI: 10.20517/mmm.2022.03

Minerals and Mineral Materials

Research Article

Open Access

Selective recovery of Pb(II) from a waste electrolyte via ion flotation with iminodiacetic acid-functionalized graphene oxide as a nanocollector

Luping Chang[1], Weijun Peng[1,2,3], Yijun Cao[1,2,3,4], Yiheng Miao[2], Guixia Fan[1], Yukun Huang[1], Xiangyu Song[1], Xianggen Chen[1]

[1]School of Chemical Engineering, Zhengzhou University, Zhengzhou 450001, Henan, China.
[2]National and Local Joint Engineering Research Center for Green Mineral Metallurgy and Processing, Zhengzhou 450001, Henan, China.
[3]Provincial and Ministerial Joint Innovation Center for Resource Materials, Zhengzhou 450001, Henan, China.
[4]Henan Province Industrial Technology Research Institute of Resources and Materials, Zhengzhou University, Zhengzhou 450001, Henan, China.

Correspondence to: Prof. Weijun Peng, School of Chemical Engineering, Zhengzhou University, No.100 Science Avenue, Zhengzhou 450001, Henan, China. E-mail: pwj@zzu.edu.cn; Dr. Yijun Cao, School of Chemical Engineering, Zhengzhou University, No.100 Science Avenue, Zhengzhou 450001, Henan, China. E-mail: yijuncao@126.com

How to cite this article: Chang L, Peng W, Cao Y, Miao Y, Fan G, Huang Y, Song X, Chen X. Selective recovery of Pb(II) from a waste electrolyte via ion flotation with iminodiacetic acid-functionalized graphene oxide as a nanocollector. *Miner Miner Mater* 2022;1:6. https://dx.doi.org/10.20517/mmm.2022.03

Received: 9 Mar 2022 **First Decision:** 14 Apr 2022 **Revised:** 20 Apr 2022 **Accepted:** 24 Apr 2022 **Published:** 11 May 2022

Academic Editor: Wencai Zhang **Copy Editor:** Fangling Lan **Production Editor:** Fangling Lan

Abstract

In this work, iminodiacetic acid-functionalized graphene oxide (IDA@GO) is prepared and used as a nanocollector for enhancing and selectively recovering Pb(II) from a strongly acidic waste electrolyte via ion flotation. IDA@GO is characterized by Fourier transform infrared spectroscopy, zeta potential measurements and atomic force microscopy. The effects of pH, reaction time, cetyl trimethyl ammonium bromide (CTAB) dosage and aeration rate on the Pb(II) concentration and turbidity of the residual solution are examined systematically. The experimental results show that the adsorption capacity of Pb(II) on IDA@GO can reach 91.21 mg/g at pH 2. After froth flotation, the turbidity of the treated solution decreased to 0.55 NTU under the optimal CTAB dosage and aeration rate. In addition, as compared with GO, the relative selectivity coefficients of IDA@GO are up to 1.304, 1.471, 1.807 and 1.509 for Co(II), Ni(II), Zn(II) and Cd(II), respectively, thereby exhibiting better selectivity performance. Moreover, IDA@GO can be reused as a nanocollector in ion flotation and exhibits ideal regeneration performance. In addition, the recovery mechanism is found to proceed through Pb(II) adsorbing on IDA@GO by electrostatic attraction, ion

exchange and surface complexation, with the addition of CTAB improving the hydrophobicity of Pb(II)-loaded IDA@GO flocs, thus achieving the recovery of Pb(II) via froth flotation.

Keywords: Nanocollector, iminodiacetic acid-functionalized graphene oxide, selectively recovery, ion flotation, Pb(II), strongly acidic waste electrolyte

INTRODUCTION

As a common metal, lead and its oxide are widely used in various industrial sectors and applications, including chemicals, cables, batteries and environmental and radioactive protection, due to their excellent physicochemical properties[1-3]. However, large amounts of waste electrolytes are inevitably generated during their production and processing. It is well known that waste electrolytes typically exist as wastewater, which may cause irreversible damage to the human body due to the mobility and non-degradability of lead ions[4-6]. Therefore, waste electrolytes should be properly treated before discharge from the perspective of environmental protection. In addition, lead in waste electrolytes is considered an important resource for economic development due to the broadening application fields, meaning that the lead ions in waste electrolytes should also be recovered as much as possible from the perspective of a circular economy[7].

Significant efforts have been devoted to the removal or selective recovery of heavy metal ions using many kinds of physicochemical methods, including adsorption[8], redox[9], chemical precipitation[10], ion exchange[11], electrodialysis[12] and leaching[13]. Although the above methods have achieved good results in the field of heavy metal wastewater treatment, they all suffer from unique disadvantages, such as high operating costs, low removal rates, large consumption of adsorbents, secondary pollution, poor selectivity and so on[14,15]. In recent years, ion flotation has been gradually applied to the treatment of heavy metal wastewater, the recovery of precious metals and the selective separation of multi-component ions, and has attracted increasing research attention due to its unique advantages, which include simple and rapid operation, high removal rates and selectivity, low operating costs, small space requirements and energy efficiency[16,17]. Ion flotation was used by Chirkst *et al.*[18] for the pre-concentration of rare earth elements. They found that Y(III) and Ce(III) could be selectively recovered by adjusting the pH of the solution to 5 and 7, respectively, indicating that ion flotation is an efficient method for the selective recovery of rare earth elements[18].

As reported previously, the collectors adopted in the process of ion flotation play a decisive role in removing or recovering metal ions[19]. The most commonly used chemically synthesized[20] and biological[21] collectors possess different fatal defects (such as large consumption, low removal rates and environmental unfriendliness), which have contributed to the emergence of nanocollectors[22]. Compared with chemically synthesized and biological collectors, nanocollectors have the advantages of lower dosages, high removal rates, shorter flotation times and recyclability, and have gradually become a research hotspot in recent years[19].

In our previous research, as a common carbon-based material[23], graphene oxide (GO) was proven to be an ideal nanocollector for heavy metal ions [such as Pb(II) and Cu(II)] removal. Furthermore, both the turbidity and chemical oxygen demand of the treated solution met the discharge standard of industrial wastewater[24]. The removal performance of heavy metal ions can also be enhanced by increasing the oxidation degree of GO[25]. However, minimal differences were found between the affinities of the oxygen-containing functional groups on the GO surface toward metal ions and the selectivity performance of GO was rather poor[26]. In order to improve the Cu(II) selectivity performance of GO in the ion flotation

process, 1,3-diamino-1,2,3-trioximido-propane, which exhibited a better affinity towards Cu(II), was adopted for the modification of GO[27]. As a result, Pb(II) recovery with high selectivity through ion flotation with GO as a nanocollector appears infeasible without modification. In addition, Pb(II)-containing waste electrolytes usually exist as strongly acidic solutions. If such a solution is adjusted to a neutral solution in the Pb(II) recovery process, a large amount of alkali will be wasted and the complexity of the operation will be increased, which will effectively remove the advantages of ion flotation. To the best of our knowledge, there have been no reports on the selective recovery of Pb(II) with modified GO as a nanocollector through ion flotation in a strongly acidic solution.

Therefore, GO and iminodiacetic acid-functionalized GO (IDA@GO) as nanocollectors for the selective recovery of Pb(II) from a strongly acidic Pb(II)-containing waste electrolyte are investigated in this study systematically. IDA@GO is synthesized and characterized by Fourier transform infrared (FT-IR) spectroscopy, zeta potential measurements and atomic force microscopy (AFM). The effects of pH, reaction time, cetyl trimethyl ammonium bromide (CTAB) dosage and aeration rate are studied in detail. Furthermore, the recovery mechanism is illustrated by FT-IR spectroscopy and zeta potential and water contact angle (WCA) measurements.

EXPERIMENTAL

Materials

Graphite powder was obtained from Sinopharm Chemical Reagent Co., Ltd. (China). Sulfuric acid (H_2SO_4), nitric acid (HNO_3), hydrochloric acid (HCl) and hydrogen peroxide (H_2O_2) of analytical grade were purchased from Luoyang Haohua Chemical Reagent Co., Ltd. (China). Sodium nitrate ($NaNO_3$) and sodium hydroxide (NaOH) of analytical grade were received from Sinopharm Chemical Reagent Co., Ltd. (China). CTAB and iminodiacetic acid of analytical grade were purchased from Shanghai Maclean Biochemical Technology Co., Ltd. (China). Deionized water was used in all experiments unless otherwise stated.

Synthesis of IDA@GO

GO powder was first synthesized by the Hummers method and the detailed operation procedure is available in our previous study[28]. A GO suspension with a certain concentration (2 mg/L) was then obtained by ultrasonic stripping. Subsequently, certain volumes of GO and IDA suspensions (1 g/L) were mixed in a three-necked flask and subjected to reflux with continuous stirring for 6 h at 60 °C. Afterwards, the reaction product was separated by centrifugation at 5000 rpm for 10 min, rinsed three times with ethanol and deionized water, respectively, and then redispersed into a certain volume of deionized water to form the homogeneous IDA@GO suspension (as shown in Scheme 1). Finally, a 20 mL IDA@GO solution was sampled and dried. The concentration of the IDA@GO solution could be calculated according to Eq. (1):

$$c_{IDA@GO} = \frac{m_2 - m_1}{20} \quad (1)$$

where $c_{IDA@GO}$ (mg/mL) represents the concentration of the IDA@GO solution and m_1 and m_2 (mg) are the masses of the empty watch glass and watch glass together with IDA@GO after drying, respectively.

Characterization of IDA@GO

An SPM-8100 microscope (Shimadzu, Japan) was used to obtain the AFM images, and the procedure of sample preparation is presented in our previous study[29]. The FT-IR spectra of IDA@GO in the absence and presence of Pb(II) and CTAB were recorded by a Nicolet iS10 spectrometer (Thermo Fisher Scientific, USA). A Zetasizer Nano ZS90 (Malvern, UK) was used to characterize the zeta potential of IDA@GO in the

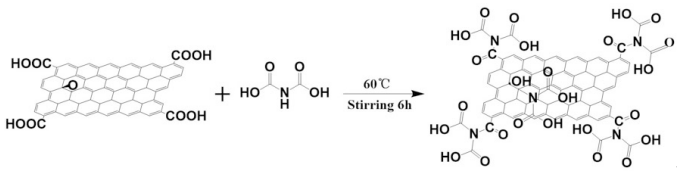

Scheme 1. Schematic of synthesis process of IDA@GO. IDA@GO: Iminodiacetic acid-functionalized graphene oxide.

absence and presence of Pb(II) and CTAB at 25 °C. A JC2000D3W instrument (Powereach, China) was obtained for the measurements of the WCA.

Pb(II) adsorption-flotation

All Pb(II) adsorption batch experiments were carried out in a 150 mL conical flask. First, a certain amount of IDA@GO solution was added to the Pb(II) stock solution and the Pb(II) concentration was set as 50 g/L. The pH value of the mixed solution was then adjusted to the desired value with the addition of a negligible volume of an HCl or NaOH solution. Afterwards, the conical flask was sealed with plastic wrap and shaken by a thermostatic oscillator (HZP-150, China) for a certain time at 150 rpm and 25 °C. The effects of pH and reaction time (0.5-2.5 or 0-120 min) were studied. After oscillation, a certain amount of CTAB was added to the solution and stirred for another 5 min. Subsequently, the mixture was transferred into a self-made flotation column equipped with a mini air compressor and rotameter, as depicted in our previous report[29]. In a batch flotation test, the foam was collected for 5 min. Finally, a certain volume of residual solution was sampled and used for Pb(II) concentration determination by Inductively Coupled Plasma Optical Emission Spectrometer (ICP-OES, Avio 500, PerkinElmer, USA) after filtering with a single-use sterile membrane filter. The adsorption capacity and recovery of Pb(II) were calculated according to Eqs. (2) and (3), respectively, and the recovery of water (enrichment ratio) was calculated using Eq. (4):

$$Q = \frac{(C_0 - C_r)V_0}{m} \tag{2}$$

$$R = \frac{C_0 - C_r}{C_0} \times 100\% \tag{3}$$

$$R_W = \frac{V_r}{V_0} \tag{4}$$

where C_0 and C_r (mg/L) are the concentrations of the initial and residual solutions, respectively, Q (mg/g) is the adsorption capacity of GO or IDA@GO, m(g) represents the weight of GO or IDA@GO and V_0 and Vr are the volumes (L) of the initial and residual solution after flotation, respectively. Finally, the flotation performance of the IDA@GO and fine flocs was also determined by a turbidimeter (TL2300, Hach, USA).

Desorption and reusability studies

For the desorption experiments, the foam product was first subjected to simple filtration to remove the water trapped by bubbles during flotation. The filter was mixed with a 20 mL HCl solution (2 mol/L) and oscillated for 2 h at 150 rpm and 25 °C. After oscillation, the mixture was centrifuged at 3000 rpm for 5 min. The supernatant was sampled for the determination of the Pb(II) concentration by ICP-OES and the desorption rate of Pb(II) was calculated according to Eq. (5):

$$D = \frac{C_d V_d}{(C_0 - C_r)V_0} \times 100\% \tag{5}$$

where C_d (mg/L) is the Cu(II) concentration of the desorption supernatant and V_d is the volume of the desorption suspension. The precipitate obtained from centrifuge was rinsed twice with ethanol and water, respectively. Afterwards, the rinsed IDA@GO was subjected to redispersion in deionized water and used for

another adsorption-flotation-desorption cycle to evaluate its reusability.

In addition, the concentration of the redispersed solution was analyzed by a turbidimeter, as reported previously[30], and the recovery of IDA@GO could be calculated easily by:

$$\varepsilon_{IDA@GO} = \frac{C_{re}V_{re}}{C_iV_0} \times 100\% \quad (6)$$

where C_i and C_{re} (mg/L) represent the concentrations of IDA@GO in the initial and redispersed solutions, respectively, and V_{re} (L) is the redispersed solution volume of IDA@GO.

Selective adsorption experiments

The selective properties of both GO and IDA@GO were evaluated by selective adsorption experiments. The selective adsorption experiment was carried out in a simulated waste electrolyte containing Pb(II), Zn(II), Cd(II), Co(II) and Zn(II) with the same ion concentration (50 mg/L at pH 2). The selective performance of GO and IDA@GO were evaluated by the distribution coefficient (D, L/g), selectivity coefficient ($\beta_{Cu(II)/M(II)}$) and the relative selectivity coefficient (β_r) according to Eqs. (7)-(9), respectively[31]:

$$D = \frac{C_i - C_f}{C_f} \times \frac{V_0}{m} \quad (7)$$

$$\beta_{Pb(II)/M(II)} = \frac{D_{Pb(II)}}{D_{M(II)}} \quad (8)$$

$$\beta_r = \frac{\beta_{IDA@GO}}{\beta_{GO}} \quad (9)$$

where C_i and C_f (mg/L) are the initial and final concentrations of metal ions, respectively, $D_{Pb(II)}$ and $D_{M(II)}$ denote the distribution coefficients of Pb(II) and other interfering metal ions, respectively, and $B_{IDA@GO}$ and β_{GO} are the selectivity coefficients of IDA@GO and GO, respectively.

RESULTS AND DISCUSSION

Characterization of IDA@GO

Figure 1 illustrates the FT-IR spectra of GO and IDA@GO. Obviously, GO exhibited several characteristic peaks at 1060, 1225, 1610 and 1720 cm^{-1}, which correspond to the stretching vibration of the C-O bond, the stretching vibration of the C-O-C bond of the epoxy groups, the C=C skeletal vibrations from non-oxidized graphitic domains and the stretching vibration of the C=O bond, respectively[32]. After modification, a new characteristic peak appeared in the spectrum of IDA@GO at 1360 cm^{-1}, which could be ascribed to the stretching vibration of the C-N bond[33]. Furthermore, the characteristic peak at 3380 cm^{-1} (stretching vibration of -OH from hydroxyl and carboxyl groups and water molecules) shifted to 3410 cm^{-1}. The intensity of the characteristic peak at 1225 cm^{-1} decreased sharply, indicating that carboxyl and epoxy groups serve as active sites for the modification[34]. In summary, IDA@GO was successfully synthesized with iminodiacetic acid as a modifier.

Figure 2 represents the surface zeta potential of IDA@GO. Obviously, IDA@GO was negatively charged in the tested pH range. Even at pH 1.02, its surface zeta potential was -30.21 mV, meaning it could interact with cation ions readily through electrostatic attraction, endowing IDA@GO with an excellent cation ion removal performance. Furthermore, the zeta potential became more negative with increasing pH due to the increase in negative charge density.

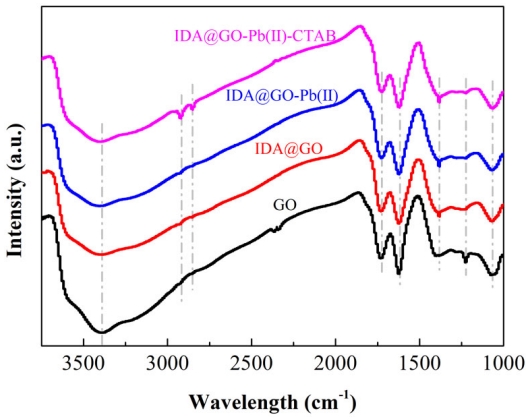

Figure 1. FT-IR spectra of GO, IDA@GO, IDA@GO-Pb(II) and IDA@GO-Pb(II)-CTAB. FT-IR: Fourier transform infrared; GO: graphene oxide; IDA@GO: iminodiacetic acid-functionalized graphene oxide; CTAB: cetyl trimethyl ammonium bromide.

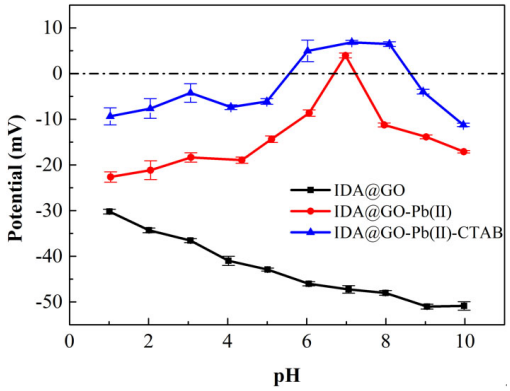

Figure 2. Zeta potentials of IDA@GO, IDA@GO-Pb(II) and IDA@GO-Pb(II)-CTAB. CTAB: Cetyl trimethyl ammonium bromide. IDA@GO: iminodiacetic acid-functionalized graphene oxide.

Figure 3 shows a representative AFM image of IDA@GO and a height map of the selected cross section. Apparently, IDA@GO still possessed a typical lamellar structure, which showed no obvious difference compared with GO. In addition, the height of the cross section along the line was ~1.2 nm, thereby meeting the size requirements of a nanocollector and illustrating the potential of IDA@GO as a nanocollector.

Recovery of Pb(II)

Effect of pH

Unlike previous research, the Pb(II)-containing waste electrolyte is a kind of strongly acidic solution. It was not cost-effective to increase the Pb(II) recovery by adding alkali to elevate the pH of the initial solution. Therefore, the recovery of Pb(II) was carried out in a strongly acidic solution. As depicted in previous studies, the pH played a critical role in the interaction between heavy metal ions and the nanocollector, with the heavy metal ion removal performance dominated by the pH of the initial solution[35]. The influence of pH of the initial solution on Pb(II) adsorption capacity was investigated and the results are shown in Figure 4. With the pH of the initial solution increased from 0.58 to 2.50, the Pb(II) adsorption capacity of IDA@GO and GO increased from 9.30 and 6.80 mg/g to 131.50 and 108.70 mg/g, respectively. The specific reasons are as follows. More H^+ existed at lower pH, which occupied the adsorption sites on IDA@GO due to protonation, resulting in strong competition between H^+ and Pb(II), leading to a lower Pb(II) uptake of IDA@GO. With increasing pH, the concentration of H^+ decreased sharply and more vacant adsorption sites appeared due to deprotonation, resulting in a higher Pb(II) adsorption capacity. With increasing pH, the

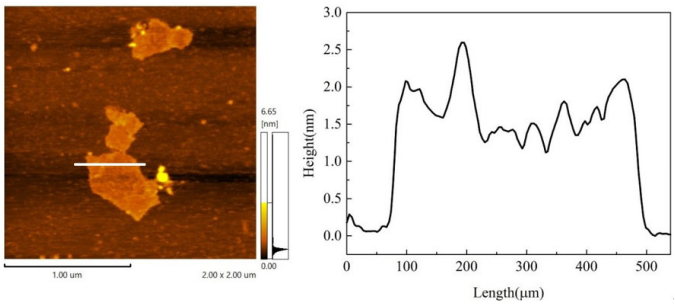

Figure 3. AFM image of IDA@GO. AFM: Atomic force microscopy; IDA@GO: iminodiacetic acid-functionalized graphene oxide.

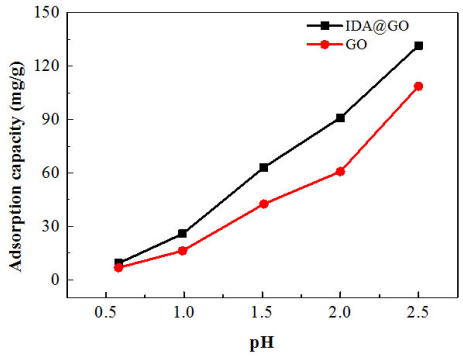

Figure 4. Pb(II) adsorption on IDA@GO and GO as a function of pH (Pb(II) concentration of 50 mg/L, GO and IDA@GO concentration of 100 mg/L and reaction time of 120 min). IDA@GO: Iminodiacetic acid-functionalized graphene oxide; GO: graphene oxide.

surface zeta potential of IDA@GO became more negative. Therefore, Pb(II) ions more readily interacted with IDA@GO due to electrostatic attraction, bringing about an enhancement in the Pb(II) adsorption capacity. In addition, it was obviously noted that IDA@GO possessed a much larger Pb(II) adsorption capacity than GO in the experimental pH range, suggesting that after modification, IDA@GO exhibited a better affinity and recovery performance than GO. For the purpose of reducing alkali consumption and ensuring Pb(II) recovery, the initial solution pH was set as 2 and was applied for further tests.

Effect of reaction time

It is well known that sufficient time is needed for the interaction between the nanocollector and the heavy metal ions, so that more heavy metal ions could be adsorbed on the nanocollector, thus achieving excellent recovery performance. In this study, the adsorption behavior of Pb(II) on IDA@GO and GO as a function of reaction time was studied and the result is shown in Figure 5. Obviously, the adsorption rate of both IDA@GO and GO exhibited a dramatic increasing trend in the first 20 min due to the presence of plentiful vacant adsorption sites. With increasing time, the vacant adsorption sites diminished gradually and the adsorption slowed down gradually and reached the adsorption equilibrium. Furthermore, the maximum Pb(II) adsorption capacities of IDA@GO and GO were 91.21 and 61.89 mg/g, respectively, demonstrating that the introduction of iminoethylene acid improved the affinity between GO and Pb(II), thereby endowing IDA@GO with a greater Pb(II) adsorption capacity. In addition, IDA@GO and GO could reach the adsorption equilibrium in 40 and 60 min, respectively, suggesting that after the modification, IDA@GO exhibited a greater adsorption capacity and quicker adsorption rate towards Pb(II). This phenomenon also agrees well with the result obtained from the pH experiment. Hence, 40 min was selected as a suitable reaction time for subsequent tests.

Effects of CTAB dosage

As reported in our previous research, CTAB is a classic cationic surfactant. When used as a foaming agent,

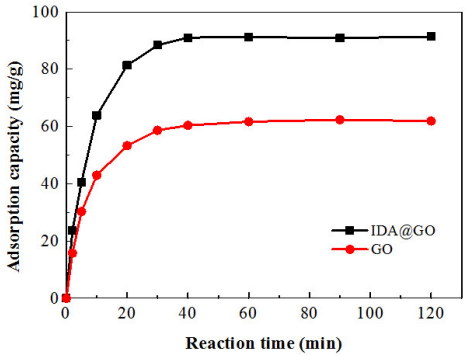

Figure 5. Effect of reaction time on adsorption of Pb(II) on IDA@GO and GO (pH 2, Pb(II) concentration of 50 mg/L and IDA@GO and GO concentration of 100 mg/L). IDA@GO: Iminodiacetic acid-functionalized graphene oxide; GO: graphene oxide.

it could not only decrease the surface tension of the solution and produce a stable foam phase, but also could interact with GO through electrostatic attraction, hydrogen bonding and surface complexation[36]. Furthermore, the hydrophobicity of GO-Cu(II) flocs is greatly improved, allowing the interaction between the flocs and bubbles to occur more readily, thereby achieving the separation of GO-Cu(II) flocs from wastewater[25]. Considering the similar physicochemical properties of GO-Cu(II) and IDA@GO-Pb(II), CTAB was selected as a foaming agent for IDA@GO-Pb(II) floc removal, thereby realizing the recovery of Pb(II) through ion flotation.

Figure 6 demonstrates the Pb(II) concentration and turbidity of the treated solution as a function of CTAB dosage. The Pb(II) concentration of the treated solution after ion flotation rarely changed, with the CTAB dosage increasing from 2.5 to 15 mg/L. This was because CTAB was a classic cationic foaming agent that barely interacted with IDA@GO because of electrostatic repulsion. Due to the hydrophilicity of IDA@GO flocs, they could not adhere to the rising bubbles generated from the bottom of the flotation column, even with sufficient collision probability. As a result, the Pb(II)-loaded flocs could not be recovered efficiently. With the CTAB dosage increased from 2.5 to 7.5 mg/g, increasingly more Pb(II)-loaded flocs were floated out, the treated solution became more clear and the turbidity of the residual solution decreased from 15.01 to 0.55 NTU rapidly, thereby realizing the recovery of Pb(II) from the waste electrolyte. This might be due to the improvement of hydrophobicity for IDA@GO-Pb(II) flocs brought by CTAB with its long carbon chain. As the dosage of CTAB increased further from 7.5 to 15 mg/L, the turbidity of the treated solution no longer changed due to the fact that almost all flocs were gathered in the foam phase with a CTAB dosage of 7.5 mg/L. In addition, the effect of CTAB dosage on water recovery (R_W) was also studied for characterizing the enrichment ratio of ion flotation and the result is also shown in Figure 6. Apparently, with increasing CTAB dosage, the surface tension of solution decreased sharply and more bubbles were easier to form. As a result, more water was entrained into bubbles and reached the foam phase, causing R_W to decrease from 95.31% to 81.23% with the CTAB dosage increasing from 2.5 to 15 mg/L. Generally, a greater R_W represents not only a higher enrichment ratio, which is advantageous for the subsequent separation of the recovered IDA@GO, but also larger amounts of treated water reused for industrial production. Therefore, 7.5 mg/L was selected as the suitable CTAB dosage for subsequent experiments.

Effect of aeration rate

The key to obtaining a large R_W is to reduce the amount of water trapped by bubbles. In ion flotation, the aeration rate should be sufficiently low to decrease the amount of water trapped by bubbles and thus achieve a dry foam product[37]. Furthermore, the aeration rate should be sufficiently high to ensure a sufficient collision probability. Therefore, the effect of aeration rate on $C_{Pb(II)}$, the turbidity of the residual solution and R_W was determined and the result is shown in Figure 7. From Figure 7, there was little change for $C_{Pb(II)}$ with the aeration rate increased from 50 to 200 mL/min, demonstrating that it has a minimal effect on Pb(II)

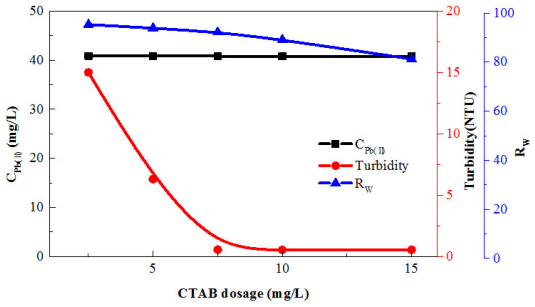

Figure 6. Effect of CTAB dosage on $C_{Pb(II)}$, turbidity of residual solution and R_W (pH 2, Pb(II) concentration of 50 mg/L, IDA@GO concentration of 100 mg/L, reaction time of 40 min and aeration rate of 100 mL/min). CTAB: Cetyl trimethyl ammonium bromide; IDA@GO: iminodiacetic acid-functionalized graphene oxide.

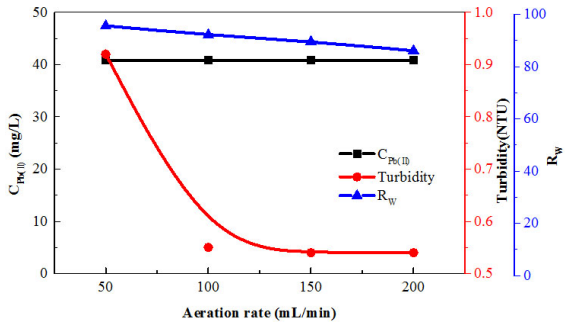

Figure 7. Effect of aeration rate on $CPb_{(II)}$, turbidity of treated solution and R_W (pH 2, Pb(II) concentration of 50 mg/L, IDA@GO concentration of 100 mg/L, reaction time of 40 min and CTAB concentration of 7.5 mg/L). IDA@GO: Iminodiacetic acid-functionalized graphene oxide; CTAB: cetyl trimethyl ammonium bromide.

recovery. However, the collision probability between bubbles and IDA@GO-Pb(II) flocs was enhanced because more bubbles were generated with an increasing aeration rate. Therefore, the turbidity of the residual solution decreased from 0.92 to 0.55 NTU with the aeration rate increased from 50 to 100 mL/min. After that, a further increase in aeration rate to 200 mL/min resulted in no change in the turbidity, indicating that a 100 mL/min aeration rate was sufficient for IDA@GO-Pb(II) floc flotation. Unlike $C_{Pb(II)}$ and the turbidity of the residual solution, R_W decreased from 95.65% to 86.12% gradually with the aeration rate increased from 50 to 200 mL/min, because more bubbles were generated and a greater volume of water was entrained into the foam phase. According to the above results and analysis, 100 mL/min was chosen as a suitable aeration rate for Pb(II) recovery through ion flotation.

Adsorption selectivity

The wastewater produced from practical industrial production always contains more than one kind of metal ion. Just like waste electrolyte, it is usually composed of Ni(II), Zn(II), Cd(II), Co(II) and Pb(II). The existence of co-existing ions may pose a detrimental effect on recovering one specific ion. Therefore, the selective adsorption properties of Pb(II) on IDA@GO were tested, with Co(II), Ni(II), Zn(II) and Cd(II) selected as interfering ions. Figure 8 displays the selective adsorption performance of multi-component ions on IDA@GO. It can be seen that with the introduction of co-existing ions, the adsorption capacity of Pb(II) on IDA@GO and GO showed a small decrease, indicating competitive adsorption between heavy metal ions. Furthermore, IDA@GO possessed a much greater Pb(II) adsorption capacity than GO whether in single-ion or multiple component adsorption. Furthermore, the adsorption capacity of co-existing ions for IDA@GO and GO exhibited no obvious difference, illustrating that IDA@GO held a better selectivity towards Pb(II). In addition, the selectivity of IDA@GO and GO were evaluated in detail by calculating the distribution, selectivity and relative selective coefficients and the results are shown in Table 1. It was noted both the distribution coefficient and selectivity coefficient for Pb(II)/M(II) (M=Co, Ni, Zn or Cd) of

Table 1. Selectivity parameters of IDA@GO and GO for Cu(II)

Ions	Distribution coefficient *D*		Selectivity coefficient $\beta_{Cu(II)/M(II)}$		Relative selectivity coefficient β_r
	IDA@GO	GO	IDA@GO	GO	
Pb(II)	20.120	12.148	-	-	-
Co(II)	0.513	0.404	39.221	30.069	1.304
Ni(II)	0.634	0.563	31.735	21.557	1.471
Zn(II)	0.438	0.478	45.934	25.414	1.807
Cd(II)	0.709	0.646	28.378	18.805	1.509

IDA@GO: Iminodiacetic acid-functionalized graphene oxide; GO: graphene oxide.

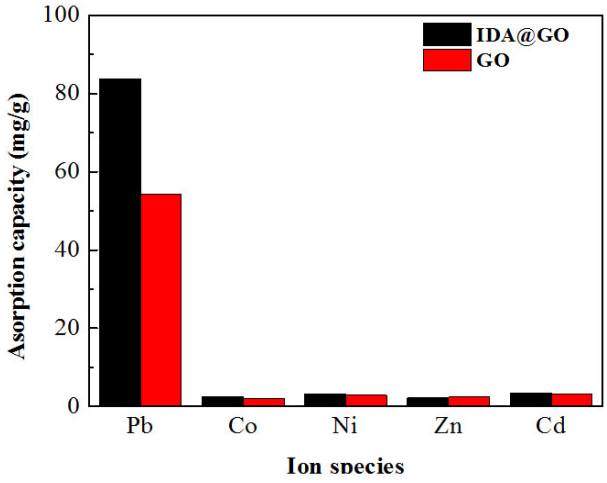

Figure 8. Selective adsorption of Pb(II) on IDA@GO and GO. IDA@GO: Iminodiacetic acid-functionalized graphene oxide; GO: graphene oxide.

IDA@GO were significantly larger than that of GO. Moreover, the relative selectivity coefficients for each heavy metal ion were much larger than 1, suggesting that iminodiacetic acid grafted on GO dramatically increased the selectivity to Pb(II) due to its better affinity towards Pb(II). Hence, IDA@GO was able to efficiently and selectively recover Pb(II) from the multi-component waste electrolyte through ion flotation.

Recovery mechanism

IDA@GO has proven to be an efficient nanocollector for Pb(II) recovery via ion flotation from the above tests. Therefore, the recovery mechanism was investigated thoroughly.

Mechanism of Pb(II) adsorption on IDA@GO

Figure 1 represents the FT-IR spectrum of Pb(II)-loaded IDA@GO. After Pb(II) adsorption, the broad peak at 3410 cm^{-1} shifted to 3429 cm^{-1}, suggesting Pb(II) was adsorbed on the oxygenous functional groups of IDA@GO by surface complexation and ion exchange. Furthermore, the intensity of the characteristic peak at 1720 cm^{-1} decreased to some extent, specifying that the carboxyl groups served as the main adsorption sites[28,38].

Figure 2 depicts the zeta potential of IDA@GO after Pb(II) adsorption. Conspicuously, the zeta potential moved to the positive direction after conditioning with Pb(II), indicating that IDA@GO could interact with Pb(II) via electrostatic attraction to achieve Pb(II) recovery.

Mechanism of flotation separation

Mechanism of interaction between CTAB and Pb(II) loaded IDA@GO

As compared with the FT-IR spectrum of IDA@GO-Pb(II), two new peaks, which could be ascribed to the -CH_2 stretching vibration (2919 cm^{-1}) and the -CH_3 stretching vibration (2840 cm^{-1}), appeared with the addition of CTAB[39]. In addition, the intensity of the peak at 1220 cm^{-1} (C-O-C stretching vibration from the epoxy group) disappeared after CTAB adsorption, specifying that CTAB was adsorbed on Pb(II)-loaded IDA@-GO with the epoxy groups as adsorption sites. The zeta potential exhibited another positive shift, suggesting that electrostatic attraction played a critical role in the interaction between CTAB and IDA@GO@Pb(II).

In mineral flotation, WCA is a reliable parameter used for revealing the recovery mechanism by evaluating the floatability of a mineral. Therefore, WCA analysis was conducted in this study. Figure 9 illustrates the WCA as the function of CTAB dosage. Notably, the WCA of Pb(II)-loaded IDA@GO was only 33.56°, displaying a hydrophilic surface, so that rare flocs could be floated out. With the dosage of CTAB increased to 7.5 mg/L, the WCA of IDA@GO-Pb(II) increased dramatically to 68.37°. After that, the WCA remained basically unchanged with a further increase in CTAB dosage. The analysis of the WCA agrees well with the result obtained from the CTAB dosage experiments. In summary, the addition of CTAB improved the surface hydrophobicity of Pb(II)-loaded IDA@GO, so that Pb(II) could be recovered via froth flotation.

As concluded from the above analysis, the mechanism for Pb(II) recovery with IDA@GO as a nanocollector through ion flotation could be concluded as follows (as shown in Scheme 2). Firstly, Pb(II) was adsorbed on IDA@GO through ion exchange, electrostatic attraction and surface complexation with carboxyl serving as adsorption sites. Furthermore, IDA@GO was flocculated into large flocs due to surface complexation, making Pb(II)-loaded IDA@GO collide with bubbles more easily. Secondly, the addition of CTAB improved the hydrophobicity of IDA@GO-Pb(II). Therefore, the IDA@GO-Pb(II) flocs were floated out easily, finally achieving the recovery of Pb(II).

Regeneration

In addition, as another important parameter, the regeneration property of the nanocollector was evaluated by carrying out consecutive adsorption-flotation-desorption experiments. It was found that when IDA@GO was used for the second adsorption-flotation-desorption experiment, its adsorption capacity towards Pb(II) was 85.21 mg/g, which maintained as high as 93.42% of the first cycle. Furthermore, the turbidity of the treated solution after the second flotation was 0.55 NTU and the recovery of IDA@GO maintained as high as 95.32% after two cycle experiments. Overall, IDA@GO holds significant potential for further practical use in removing and recovering Pb(II) from strongly acidic waste electrolytes.

CONCLUSION

In this work, IDA@GO was successfully synthesized and employed as a nanocollector for selectively recovering Pb(II) from a strongly acidic waste electrolyte via ion flotation. The results suggested that IDA@GO exhibited superior performance for the recovery of Pb(II) than GO on behalf of higher adsorption capacity and quicker adsorption rate. About 91.21 mg/g of Pb(II) could be recovered from synthetic waste electrolyte effectively with a 0.55 NTU turbidity of the residual solution. Compared with GO, IDA@GO showed a better selectivity towards Pb(II) with relative selectivity coefficients of 1.304, 1.471, 1.807 and 1.509 for Co(II), Ni(II), Zn(II) and Cd(II), respectively. In addition, IDA@GO exhibited an ideal recycling performance. In addition, the recovery mechanism was proven to be Pb(II) adsorption via electrostatic attraction, hydrogen bonding and surface complexation accompanied by CTAB improving the hydrophobicity to isolate the flocs from the aqueous solution.

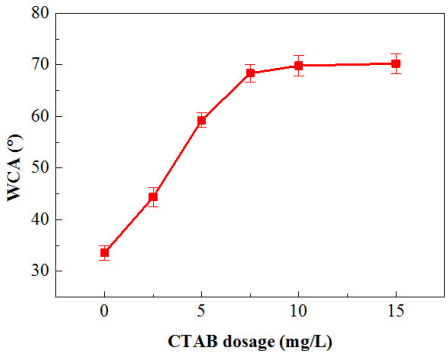

Figure 9. Effect of CTAB concentration on WCA of IDA@GO-Pb(II). CTAB: Cetyl trimethyl ammonium bromide; WCA: water contact angle; IDA@GO: iminodiacetic acid-functionalized graphene oxide.

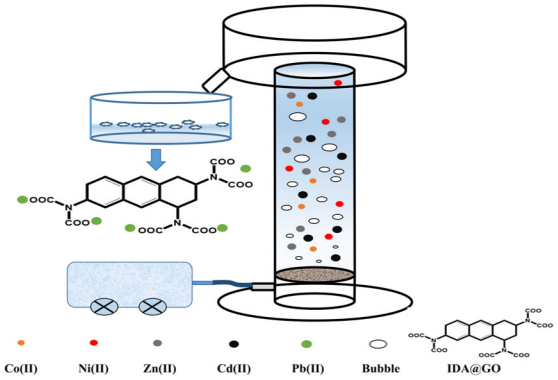

Scheme 2. Schematic for selective recovery of Pb(II) with IDA@GO as a nanocollector via ion flotation. IDA@GO: Iminodiacetic acid-functionalized graphene oxide.

DECLARATIONS

Authors' contributions

Conceptualization, Funding acquisition, Writing - review & editing: Peng W
Conceptualization, Investigation, Formal analysis, Writing - original draft: Chang L
Conceptualization, Funding acquisition, Writing - review & editing: Cao Y
Investigation, Formal analysis: Miao Y
Writing - review & editing: Fan G, Huang Y, Song X, Chen X

Availability of data and materials

Not applicable.

Financial support and sponsorship

The authors gratefully acknowledge the financial support from the National Natural Science Foundation of China (project No. 51804275, U1704252, 51904275 and 51874259), the National key research and development program (NO. 2018YFC0604702, 2018YFC1901601). Moreover, we also thank Program for Innovative Research Team (in Science and Technology) in University of Henan Province (NO. 19IRTSTHN028), China Postdoctoral Science Foundation (No. 2018M632811, 2019T120638 and 2020T130612), Key scientific research project plan of Henan colleges and universities (No.19A45001), Science and Technology project of Henan Province (192102310246) and Modern Analysis and Gene Sequencing Centre in Zhengzhou University.

Conflicts of interest

The authors declare that they have no known competing financial interests or personal relationships that could have appeared to influence the work reported in this paper.

Ethical approval and consent to participate

Not applicable.

Consent for publication

Not applicable.

Copyright

REFERENCES

1. Masoomi MY, Bagheri M, Morsali A. Porosity and dye adsorption enhancement by ultrasonic synthesized Cd(II) based metal-organic framework. *Ultrason Sonochem* 2017;37:244-50. DOI PubMed
2. Abu-Danso E, Peräniemi S, Leiviskä T, Bhatnagar A. Synthesis of S-ligand tethered cellulose nanofibers for efficient removal of Pb(II) and Cd(II) ions from synthetic and industrial wastewater. *Environ Pollut* 2018;242:1988-97. DOI PubMed
3. Han N, Zhao X, Thakur VK. Adjusting the interfacial adhesion via surface modification to prepare high-performance fibers. *Nano Mater Sci* 2021. DOI
4. Peng Y, Zhang S, Zhong Q, et al. Removal of heavy metals from abandoned smelter contaminated soil with poly-phosphonic acid: Two-objective optimization based on washing efficiency and risk assessment. *Chem Eng J* 2021;421:129882. DOI
5. Harvey PJ, Handley HK, Taylor MP. Widespread copper and lead contamination of household drinking water, New South Wales, Australia. *Environ Res* 2016;151:275-85. DOI PubMed
6. Cheng H, Hu Y. Lead (Pb) isotopic fingerprinting and its applications in lead pollution studies in China: a review. *Environ Pollut* 2010;158:1134-46. DOI PubMed
7. Jamali A, Tehrani AA, Shemirani F, Morsali A. Lanthanide metal-organic frameworks as selective microporous materials for adsorption of heavy metal ions. *Dalton Trans* 2016;45:9193-200. DOI PubMed
8. Luo J, Sun M, Ritt CL, et al. Tuning Pb(II) Adsorption from Aqueous Solutions on Ultrathin Iron Oxychloride (FeOCl) Nanosheets. *Environ Sci Technol* 2019;53:2075-85. DOI PubMed
9. Liu T, Lawluvy Y, Shi Y, et al. Adsorption of cadmium and lead from aqueous solution using modified biochar: A review. *J Environ Chem Eng* 2022;10:106502. DOI
10. Xue ZF, Cheng WC, Wang L, Hu W. Effects of bacterial inoculation and calcium source on microbial-induced carbonate precipitation for lead remediation. *J Hazard Mater* 2022;426:128090. DOI PubMed
11. Bezzina JP, Ruder LR, Dawson R, Ogden MD. Ion exchange removal of Cu(II), Fe(II), Pb(II) and Zn(II) from acid extracted sewage sludge - Resin screening in weak acid media. *Water Res* 2019;158:257-67. DOI PubMed
12. Chen S, Zhu J, Li P, Sun Y, Yang M, Huang X. In-situ growth of zero-valent iron in FeOx/Mn3O4 to improve the surficial redox for high-efficient electrocatalysis of Pb(II). *Chem Eng J* 2022;430:132959. DOI
13. Sun R, Gao Y, Yang Y. Leaching of heavy metals from lead-zinc mine tailings and the subsequent migration and transformation characteristics in paddy soil. *Chemosphere* 2022;291:132792. DOI PubMed
14. Sun Y, Yin W, Wang Y, et al. Fabrication of ultra-thin MgAl layered double oxide by cellulose templating and its immobilization effect toward heavy metal ions: cation-exchange and deposition mechanism. *Chem Eng J* 2022;427:132017. DOI
15. Wang RD, He L, Zhu RR, et al. Highly efficient and selective capture Pb(II) through a novel metal-organic framework containing bifunctional groups. *J Hazard Mater* 2022;427:127852. DOI PubMed
16. Chang L, Cao Y, Fan G, Li C, Peng W. A review of the applications of ion floatation: wastewater treatment, mineral beneficiation and hydrometallurgy. *RSC Adv* 2019;9:20226-39. DOI
17. Sebba F. Concentration by Ion Flotation. *Nature* 1959;184:1062-3. DOI
18. Chirkst DE, Lobacheva OL, Berlinskii IV, Sulimova MA. Recovery and separation of Ce3+ and Y3+ ions from aqueous solutions by ion flotation. *Russ J Appl Chem* 2009;82:1370-4. DOI
19. Peng W, Chang L, Li P, Han G, Huang Y, Cao Y. An overview on the surfactants used in ion flotation. *J Mol Liq* 2019;286:110955. DOI
20. Youssef HM, Azzam MA. Efficient removal of aluminium(III) from aqueous solutions via ion-flotation technique using aluminon as a chelating agent and oleic acid as a surfactant. *Int J Environ Anal Chem* 2021:1-18. DOI
21. Jia K, Yi Y, Ma W, et al. Ion flotation of heavy metal ions by using biodegradable biosurfactant as collector: Application and removal mechanism. *Miner Eng* 2022;176:107338. DOI
22. Micheau C, Dedovets D, Bauduin P, Diat O, Girard L. Nanoparticle foam flotation for caesium decontamination using a pH-sensitive

surfactant. *Environ Sci Nano* 2019;6:1576-84. DOI

23. Han N, Guo X, Cheng J, et al. Inhibiting in situ phase transition in Ruddlesden-Popper perovskite via tailoring bond hybridization and its application in oxygen permeation. *Matter* 2021;4:1720-34. DOI
24. Peng W, Han G, Cao Y, Sun K, Song S. Efficiently removing Pb(II) from wastewater by graphene oxide using foam flotation. *Colloids Surf A Physicochem Eng Asp* 2018;556:266-72. DOI
25. Chang L, Cao Y, Peng W, et al. Enhancing the ion flotation removal of Cu(□) via regulating the oxidation degree of nano collector-graphene oxide. *J Clean Prod* 2021;295:126397. DOI
26. Lingamdinne LP, Koduru JR, Roh H, Choi Y, Chang Y, Yang J. Adsorption removal of Co(II) from waste-water using graphene oxide. *Hydrometallurgy* 2016;165:90-6. DOI
27. Chang L, Cao Y, Peng W, et al. Highly efficient and selective recovery of Cu(II) from wastewater via ion flotation with amidoxime functionalized graphene oxide as nano collector. *Sep Purif Technol* 2021;279:119674. DOI
28. Peng W, Li H, Liu Y, Song S. Comparison of Pb(II) adsorption onto graphene oxide prepared from natural graphites: Diagramming the Pb(II) adsorption sites. *Appl Surf Sci* 2016;364:620-7. DOI
29. Chang L, Cao Y, Peng W, et al. Insight into the effect of oxidation degree of graphene oxides on their removal from wastewater via froth flotation. *Chemosphere* 2021;262:127837. DOI PubMed
30. Khlebtsov BN, Khanadeev VA, Khlebtsov NG. Determination of the size, concentration, and refractive index of silica nanoparticles from turbidity spectra. *Langmuir* 2008;24:8964-70. DOI PubMed
31. Zouboulis A. Silver recovery from aqueous streams using ion flotation. *Miner Eng* 1995;8:1477-88. DOI
32. Fang P, Xia W, Zhou Y, et al. Ion-imprinted mesoporous silica/magnetic graphene oxide composites functionalized with Schiff-base for selective Cu(II) capture and simultaneously being transformed as a robust heterogeneous catalyst. *Chem Eng J* 2020;385:123847. DOI
33. Meng C, Chen Q, Li X, Liu H. Controlling covalent functionalization of graphene oxide membranes to improve enantioseparation performances. *J Membr Sci* 2019;582:83-90. DOI
34. Wu Z, Gao L, Wang J, et al. Preparation of glycine mediated graphene oxide/g-C3N4 lamellar membranes for nanofiltration. *J Membr Sci* 2020;601:117948. DOI
35. Mahmoud MR, Lazaridis NK, Matis KA. Study of flotation conditions for cadmium(II) removal from aqueous solutions. *Process Saf Environ Prot* 2015;94:203-11. DOI
36. Chang L, Cao Y, Peng W, et al. Efficiently removing cetyl trimethyl ammonium bromide from wastewater by graphene oxide. *Surf Interface Anal* 2020;52:611-9. DOI
37. Hu N, Liu W, Jin L, et al. Recovery of trace Cu 2+ using a process of nano-adsorption coupled with flotation: SNP as an adsorbing carrier. *Sep Purif Technol* 2017;184:257-63. DOI
38. Han R, Lu Z, Zou W, Daotong W, Shi J, Jiujun Y. Removal of copper(II) and lead(II) from aqueous solution by manganese oxide coated sand II. Equilibrium study and competitive adsorption. *J Hazard Mater* 2006;137:480-8. DOI PubMed
39. Meng C, Sheng Y, Chen Q, Tan H, Liu H. Exceptional chiral separation of amino acid modified graphene oxide membranes with high-flux. *J Membr Sci* 2017;526:25-31. DOI